ACADÉMIE DES SCIENCES
INSTITUT DE FRANCE

*Comptes Rendus. Géoscience — Sciences de la Planète*
**2024**, Vol. 356, p. 195-209
https://doi.org/10.5802/crgeos.280

Research article

# First in situ calcite U–Pb dating revealing the past episodes of the 2019 Le Teil Earthquake (France)

**Aude Gébelin**[*,a], **Christophe Matonti**[b], **Christophe Larroque**[b,c], **Patrick Carr**[a] **and Jean-Paul Ampuero**[b]

[a] Université de Lorraine, UMR CNRS 7359, GeoRessources, F-54506 Vandœuvre-lès-Nancy, France

[b] Géoazur, Univ. Côte d'Azur, CNRS, Observatoire de la Côte d'Azur, IRD, Valbonne, France

[c] Université de Reims Champagne-Ardenne, GEGENA UR3795, Reims, France

*E-mail:* aude.gebelin@univ-lorraine.fr (A. Gébelin)

**Abstract.** In the Rhône Valley near the city of Montélimar, a Mw 4.9 surface-rupturing earthquake occurring on the 11th of November 2019 was linked to the reactivation of the NE–SW trending normal La Rouvière fault as a reverse fault mechanism. Here, we present the first in situ calcite U–Pb data acquired on well-characterized microstructures from core samples from a first exploratory drilling conducted in the NE part of the La Rouvière fault. In agreement with relative chronology data based on microstructural observations, our results allow us to define four main tectonic events: A first event from ~90 to 75 interpreted to reflect a thermal subsidence at the regional scale (Ardèche—South-East basin of France), a second event bracketed between ~60 to 50 Ma related to the N–S trending shortening of the South-East basin, a third tectonic event dated from ~40 to 37 Ma that we interpret to reflect the opening of the Gulf of Lion and European Cenozoic Rift System (ECRIS), and a fourth and final event at ~25 Ma that very likely represents a middle to late stage of the ECRIS. No more recent event has been identified on this fault.

**Keywords.** Le Teil earthquake, La Rouvière fault, U–Pb geochronology, Calcite veins, Pyrite crystals.

**Funding.** Observatoire de la Côte d'Azur, CNRS/INSU project Tellus FREMTEIL.

*Manuscript received 17 July 2024, revised 5 November 2024, accepted 19 November 2024.*

## 1. Introduction

The Mw 4.9 earthquake that occurred on the 11th of November 2019 near Montélimar, at the western side of the South-East basin of France, with a focal depth in the range of 1.0–1.3 km, produced a 4.5-km-long surface rupture (Figure 1) and strong ground motions in the epicentral area that were unexpected in such a low deformation rate plate interior [Ritz et al., 2020, Causse et al., 2021]. This earthquake, damaging many buildings and injuring people in Le Teil village, reinforces the idea that the NE–SW trending La Rouvière fault (LRF), belonging to the Cévennes faults system, is still active. Following this event, many geophysical research projects have been undertaken [e.g. Ritz et al., 2020, Delouis et al., 2021, Causse et al., 2021] to characterize and determine the epicenter and depth of the rupture. However, none of them have focused on rock mechanics, past deformation, fluid-rock-deformation interactions, or physical and chemical conditions. Our long-term project is to drill at hypocentral depth with the goal of (1) examine in detail the above aspects of this very shallow seismogenic zone, and (2) correlate the structure and mineralogy of the fault zone with their seismological behavior [e.g. Boullier, 2011],

[*] Corresponding author

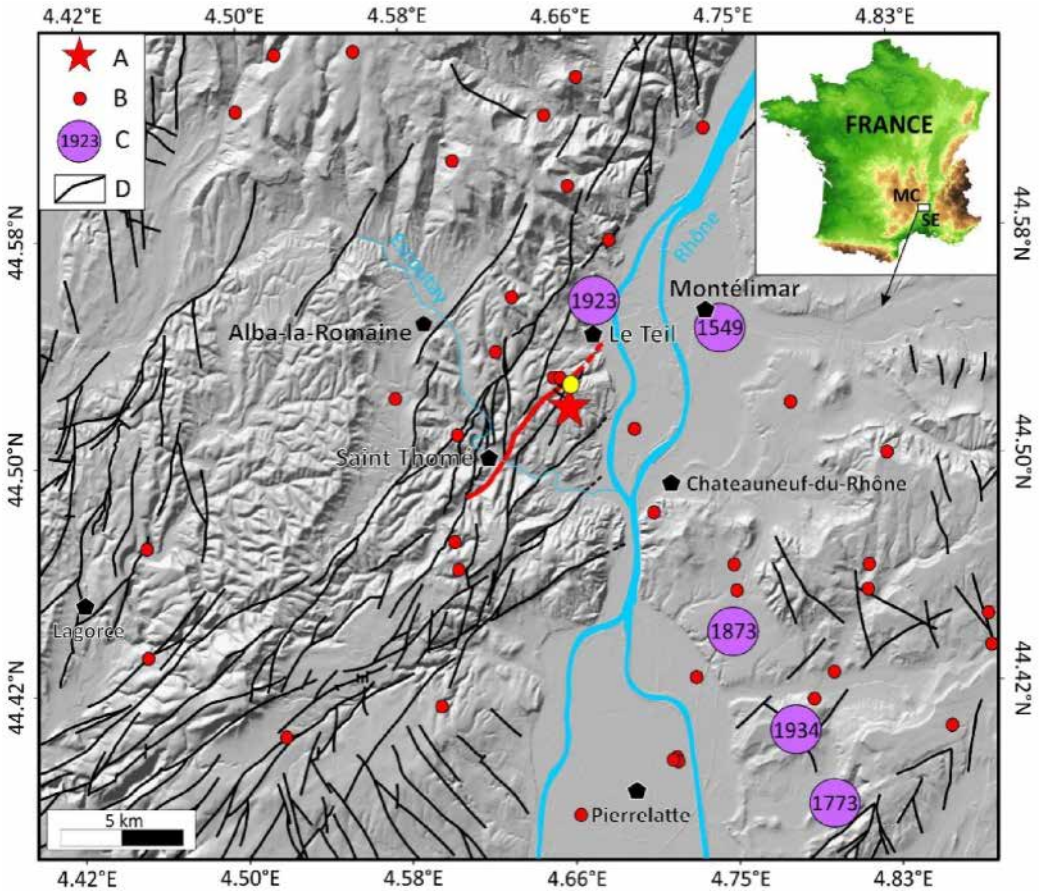


**Figure 1.** The northern Cévennes Faults system at the boundary between the Massif Central and the South-East basin of France. (A) Epicenter of the 2019-11-11 Le Teil earthquake [Delouis et al., 2021], (B) instrumental seismicity (1962–2018, https://renass.unistra.fr/instrumental-seismicity-in-mainland-france/), (C) Historical seismicity [https://www.sisfrance.net/, Jomard et al., 2021], (D) faults (http://infoterre.brgm.fr/page/telechargement-cartes-geologiques), in red: La Rouvière fault (LRF). Inset: MC: Massif Central, SE: South-East basin. The yellow circle corresponds to the drilling location.

based on samples collected from the rupture depth initiation up to the surface (Hyperdrill project, PI J. P. Ampuero, pers. Comm.). To argue the feasibility and interest of such a large-scale project, our first step was to carry out an exploratory drilling in the NE part of the fault (Figure 1 and Supplementary Figure 1) which was located at ~10 m away from the surface rupture n° 1 (44.5306° N–04.6690° E) observed by Ritz et al. [2020]. The drill crossed the fault at 20 m depth and core samples were taken from the surface down to 25.50 m depth. However, due to technical conditions the cores were not continuous, and it was clearly not possible to identify the principal slip zone of the 2019 rupture. Nevertheless, in the northeastern part of the rupture, the coseismic displacement is estimated at ~10 cm [Ritz et al., 2020]. We have identified large and localized water loss in the breccia zone within the drill core which could reflect a recent destructuration along a slip zone. However, we cannot rule out the possibility that this water loss is related to pre-existing karstic fracture.

Here, we focus on the LRF zone that is characterized by a ~3 m-thick calcareous breccia showing numerous recrystallized calcite veins and to a lesser extent some pyrite-filled fractures. Based on the

identification of key carbonate recrystallizations and microstructural observations, this paper presents the first U–Pb in situ calcite geochronological data that constrains the timing of tectonic episodes along the northern Cévennes faults system and the structural heritage of the active LRF.

## 2. Geological and seismotectonic context of the La Rouvière fault

Field, seismological and geodetical data attest that Le Teil earthquake occurred on the LRF [Ritz et al., 2020, De Novellis et al., 2020, Vallage et al., 2021, Marconato et al., 2022]. This fault belongs to the north-eastern tip of the NE–SW trending Cévennes faults system (CFS) that can be followed over more than 100 km from Montpellier to Valence, and separates the Massif Central Paleozoic crystalline basement to the west from the Meso-Cenozoic sedimentary Provence Basin to the east [Figure 1; Elmi et al., 1996]. This foreland basin, bounded by the Rhône Valley on its western side, is located west of the Alpine belt including the sub-alpine front and Penninic frontal thrust, located at ∼50 and ∼150 km from the CFS, respectively. Reverse faulting and folding have been reported in the late Miocene molasses of the Rhône Valley and are considered to be the westernmost evidences of E–W compressive stress related to the Alpine orogenesis in the area [Blès and Gros, 1991, Roure et al., 1994]. Regarding the CFS to which the LRF belongs, it underwent several tectonic episodes since the end of the Paleozoic [Roure et al., 1992, Bonijoly et al., 1996]. The 10-km-long LRF extends from the SW of the Escoutay Valley to the NE (Rhône Valley), and strikes N45E ± 5° with a dip of 55° SE ± 5° (Figure 1). It was activated by extensional tectonic during the Oligocene as a result of the Mediterranean sea opening [Séranne, 1999]. This major event is well identified in seismic reflexion profiles acquired along the Escoutay Valley where a normal offset of up to 200 m can be measured [Thomasset et al., 2024], but also in the field, where the LRF scarp marks the geomorphology.

Instrumental seismicity was sparse in the Le Teil area before the 2019 rupture. However, within a radius of 20 km around Le Teil village, only 39 earthquakes with a local magnitude lower than 2.9 have been detected between 1962 and 2018 (from ReNaSS and LDG catalogs, Figure 1). Also, several historical events occurred nearby with macroseismic intensities up to VII MSK in 1773, 1873 and 1934 for instance [Manchuel et al., 2017, Larroque et al., 2021]. Therefore, the unexpected 2019 Le Teil earthquake occurred on the unsuspected active LRF [Jomard et al., 2017] and remains the strongest event known in the area. Also, it is the first time in metropolitan France that an earthquake is clearly related to a known fault from surface ruptures observations. The moment magnitude (4.9) was moderate but large ground accelerations [>1 g in some places; Causse et al., 2021] were suspected, making the scientists convinced that the focal depth was particularly shallow [1.0–1.3 km; Delouis et al., 2021]. The focal mechanism was purely reverse with nodal planes parallel to the trace of LRF and to the alignment of surface ruptures, making the Le Teil earthquake unique as no evidence of cumulative tectonic inversion related to previous reverse earthquakes has been found so far [Ritz et al., 2020, Marconato et al., 2022].

Currently, no horizontal motion is detected from the Global Navigation Satellite Systems (GNSS) at the boundary between the Massif Central and the South-East basin. Nevertheless from a precise analysis of 20 years of continuous geodetic data, Masson et al. [2019] evidenced a NW-SE compressional strain rate of $0.7 \times 10^{-9}$ yr$^{-1}$, typical of a very low intraplate deformation rate. The 2019 reverse faulting earthquake is interpreted to reflect a tectonic inversion of the La Rouvière normal fault [Ritz et al., 2020, Marconato et al., 2022].

## 3. Samples description

### 3.1. *Macroscale structures*

The lithologies encountered in this drill hole correspond to a succession of sedimentary layers of early Cretaceous age including sands, clays and marly limestones followed by a grey calcareous breccia occurring within the 20.80 m and 23.00 m depth intervals that lies on top of massive beige limestone (Supplementary Figures 1 and 2). At 21 m depth, the breccia is cut by a gouge of less than 1 cm thick.

Here, we focus on the ∼4 m thick LRF zone that could be divided into two domains: (1) a damage zone where rocks are affected by multiple generations of open fractures and veins and, to a lesser extent, by pyrite-filled fractures (see below EC2 sample), and (2) a ∼3 m thick fault core characterized by

a calcareous breccia, and a 1 cm thick gouge band in its central part (Supplementary Figures 1 and 2).

Most fractures and veins are crosscut by numerous tectonic stylolithes of variable dip (e.g. EC3 sample in Supplementary Figure 2). The matrix alternates from a dark initial rock texture to a more beige colored texture giving the rock a macroscopically flecked aspect (e.g. EC5 sample in Supplementary Figure 2). These heterogeneities emphasize the polyphase feature of this sampled fault breccia. The first phase of brecciation consists of centimeter-to-decimeter scale angular clasts embedded in a matrix made of fine dark grey calcitic material (EC1 and EC2 samples in Supplementary Figure 2). This breccia (from herein referred to as breccia 1) characterises the upper part of the core and is then reworked as clasts during a second fluid-assisted brecciation event well observed going down the borehole and especially at the 22.5 m depth interval where a typical jigsaw geometry characterizes the core samples ("breccia 2", EC3 sample in Supplementary Figure 2). Here, a light brownish matrix is well represented and fragments are well individualized. This chaotic [sensu Mort and Woodcock, 2008] matrix supported breccia is even more pronounced going down section embedding dark grey fragments from breccia 1 (EC5 sample in Supplementary Figure 2). Although the majority of fragments are angular, some of them display rounded corners that could be due to a combination of pressure fluctuation, chemical and physical processes [Jébrak, 1997]. The light brown breccia matrix is affected by numerous stylolithes, and consists of a mixture of finely crushed breccia 1 and non-cohesive sedimentary material percolating through the porous space created from fracture opening and dilatancy processes.

### 3.2. *Microscale structures*

We focused our attention on 5 representative samples EC1 (21 m), EC2 (22 m), EC3 (22,20 m), EC4 (22,50 m) and EC5 (24 m) homogeneously distributed over the ~3 m of core drilling (Supplementary Figures 1 and 2). To characterize the sedimentary facies and the paragenesis of the deformation markers and their crosscutting relationships, thin sections were made for each sample and studied using an optical microscope. In addition, optical cathodoluminescence (CL; NewTec Scientific Cathodyne©) was used to precisely identify the successive phases of calcite (re)crystallization (with possible calcite zoning) and cements in fractures/veins as well as in interclast spaces of brecciated samples.

Using optical microscopy and CL, several phases of deformation and cementation, part of the so-called structural diagenesis [Laubach et al., 2010], can be identified in both the damage zone and the fault core. In the damage zone, we distinguish two main vein families. We first identify a tens-to-hundreds of microns wide fracture family filled with multiple anisopachous fringes/bands of small sparitic to micritic material (Fr1, Figure 2A) that we interpret to have formed from speletothem-like processes in vadose environment (lower arrow, Figure 2A and inset) [e.g. Scholle and Ulmer-Scholle, 2003]. These fractures are sometimes reactivated in opening mode, allowing for larger (>50 μm) sparite cement to fill the newly opened fracture space (upper arrow, Figure 2A). Both of these Fr1 calcite fillings display a dull blue to orange luminescence in CL (Figure 2B). We note that the associated sedimentary micritic matrix is affected by partial recrystallization occuring over millimeter-to-centimeter scale areas (upper left arrow, Figure 2C). In some places, micrite crystals are replaced by a large mosaic sparite fabric highlighted by contrasted luminescence in CL, with colours from dark blue to bright orange (Figure 2D).

This first Fr1 fracture family is crosscut by a second Fr2 fracture family whose veins are linear and of variable thicknesses (Figure 2E). In CL, these Fr2 fractures/veins are easily recognizable by their orange luminescence (Figure 2F). Two successive infilling materials characterized these Fr2 fractures: (1) fine granular material, likely originating from the breccia 2 matrix, is commonly observed on the fracture wall (arrows in Figures 2E and 2F), and (2) large sparite crystals packing the remaining fracture space correspond to the main infilling material of these fractures (Fr2 on the top right of Figures 2E and 2F).

Fr1 and Fr2 are very often crosscut by pervasive stylolites planes (Figures 2G and 2H). This deformation phase is also evidenced by the occurrence of sheared stylolites (Supplementary Figure 3) and sigmoidal en-echelon calcite vein arrays that formed through pressure solution at the restraining bends of pre-existing fractures (Figure 2C and Supplementary Figure 3).

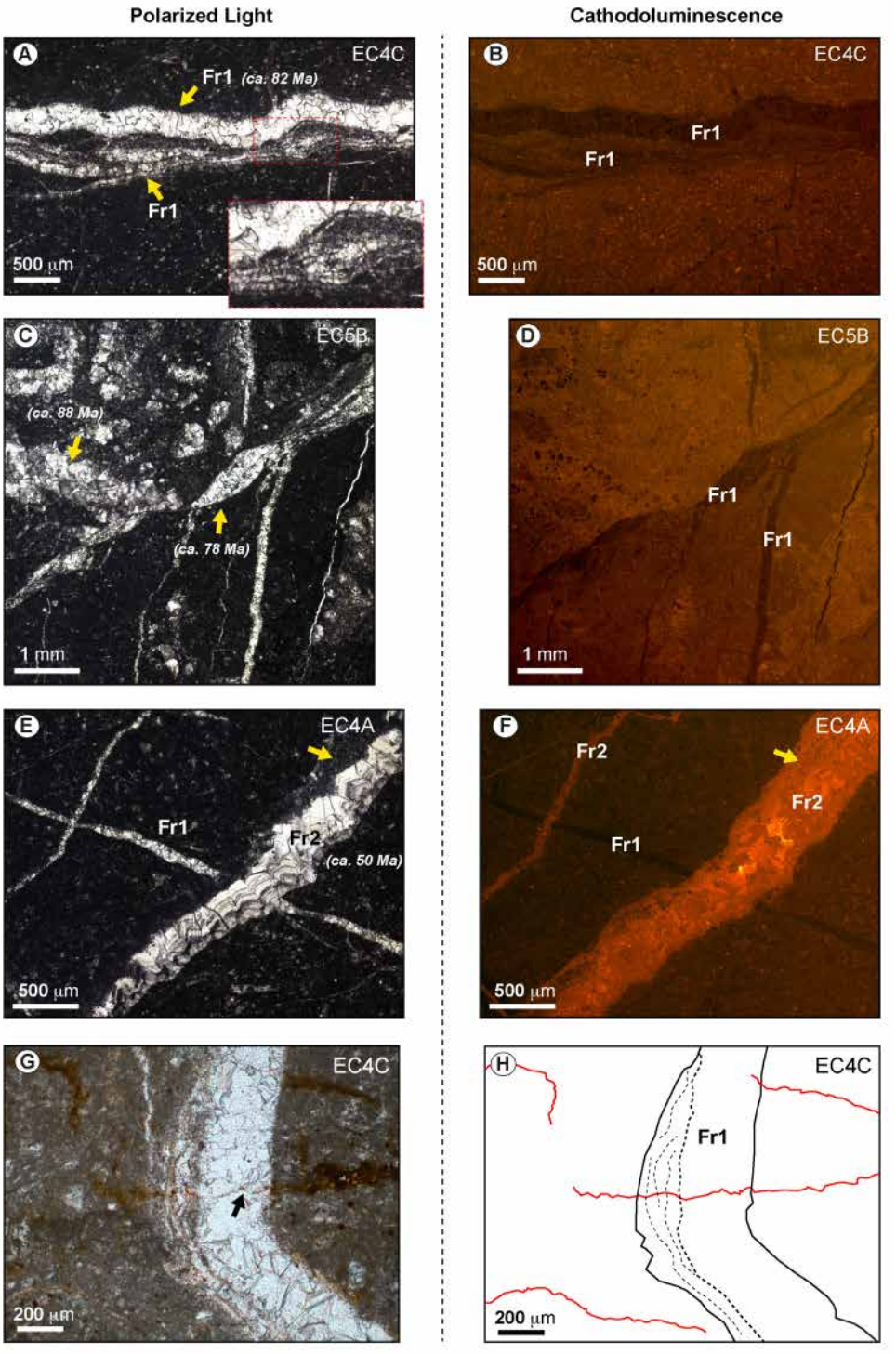


**Figure 2.** Caption continued on next page.

**Figure 2.** (**cont**.) Microphotographs of thin sections from samples of the La Rouvière Fault Damage zone. Left panels column are views in polarized light, right column are the same areas observed in cathodoluminescence (CL). (A) Fr1 fracture displaying their complex infilling originating from 2 opening events. (insert) Close-up on the anisopachous vadose calcitic infilling, (B) CL image showing the dull-luminescence of the infillings of Fr1, (C) EC5B thin section illustrating areas of recrystallized micrite, and the partially dissolved and sheared Fr1; (D) similar to C but in CL, (E) Crosscutting relationship between Fr1 and Fr2 which is characterized by 2 different infillings; (F) CL image showing the bright luminescence of Fr2 fractures compared to Fr1; (G) Crosscutting relationship between Fr1 fracture and a stylolithe plane; (H) interpretative scheme of the G panel. Note that U–Pb ages obtained in this study have been added on photographs for clarity.

In the fault core, the two main phases of brecciation are well observed at the microscopic scale (Samples EC1, EC2 and partially EC3, Figures 3A and 3B). As suspected at the macroscopic scale, the proportion of angular clasts is higher in breccia 1 (e.g. EC1 and EC2 samples in Supplementary Figures 2 and 4) than in breccia 2 (EC5 in Supplementary Figure 2). In addition to the presence of more rounded clasts, the matrix in breccia 2 is characterized by pervasive micro-stylolithes, concavo-convex clast contact (Supplementary Figure 3), as well as compaction and/or shear bands that developed as a consequence of pressure solution (Figure 3A and EC1 sample in Supplementary Figure 2 and 3). This matrix is also characterized by the presence of iron and possibly clay minerals (Figure 3A), whose presence could be associated with pressure solution processes, increasing the ratio of non-soluble over initial calcitic material. This breccia 2 matrix is also observed in non-brecciated areas, injected into re-opened fractures and dilatant zones (EC3 sample in Supplementary Figure 2, and arrows in Supplementary Figure 3).

At the ~22 m depth interval, the breccia 1 type core sample (EC2) is affected by a main fracture with a (sigmoidal shape) opening space that seems to crosscut both breccias 1 and 2 (Figures 3C, 3D and 3E and Supplementary Figure 2). We interpret this fracture to be syn-to post-breccia 2 (see above and Figure 2C). This EC2 fracture displays a millimeter-sized opening filled with calcite crystals nucleating on the fracture wall (Figure 3C). Observations in CL (Figure 3E) and under cross-polarized light (Figure 3F) highlight successive growing episodes of this syntaxial vein. From the wallrock to the median line, we can see a fringe of small calcite crystals (20 μm < size < 50 μm) overlain by larger (~100 μm) tooth shape calcite crystals ("Dog-tooth core" in Figures 3E and 3F). In CL, both crystal types are characterized by a dull orange luminescence suggesting that they formed at the same time (Figure 3E). In addition, a fringe of bright orange calcite overlies each of the large dog-tooth shape crystals ("Dog-tooth rim" in Figures 3E and 3F). This new growing episode forms a continuous rim that can reach up to 200 μm in thickness (Figure 3E). Also, the presence of pyrite grains growing on the top of this zoning calcite area (Figures 3D and 3G) indicates that chemically different fluids have circulated through this EC2 sample. In addition to the zoned calcite minerals, different observations made from the pyrite grains analysis allows us to confirm the presence of different signatures of fluids in the fault system: (1) zonation areas revealed in pyrite grains using reflected light, and electron microprobe analyses (Supplementary Figures 4 and 5 and Supplementary Table 2), (2) local fine fragmentation of pyrite crystals possibly related to fluid overpressure during faulting (Figure 3D), and (3) reprecipitation of tiny pyrite grains along calcite veins (Figures 3D and 3G) forming an angle of ~25°–30° with the main fracture surface (Figure 3F), and/or at the boundary between the host breccia rock and the first calcite generation (Figure 3G). As suspected from previous observations and cross-cutting relationships, this sample clearly reveals a polyphase history of the LRF zone.

Following up these two brecciation events, a main last phase of fracturing Fr3, cross-cutting all the above described structures, is well observed in the fault core samples (Figure 3A). These Fr3 features are distinguished in CL where they appear as a bright orange colour (Figure 3B). This third event is also recognizable by the presence of more or less tortuous fractures (Figure 3B) filled with altered subhedral micro

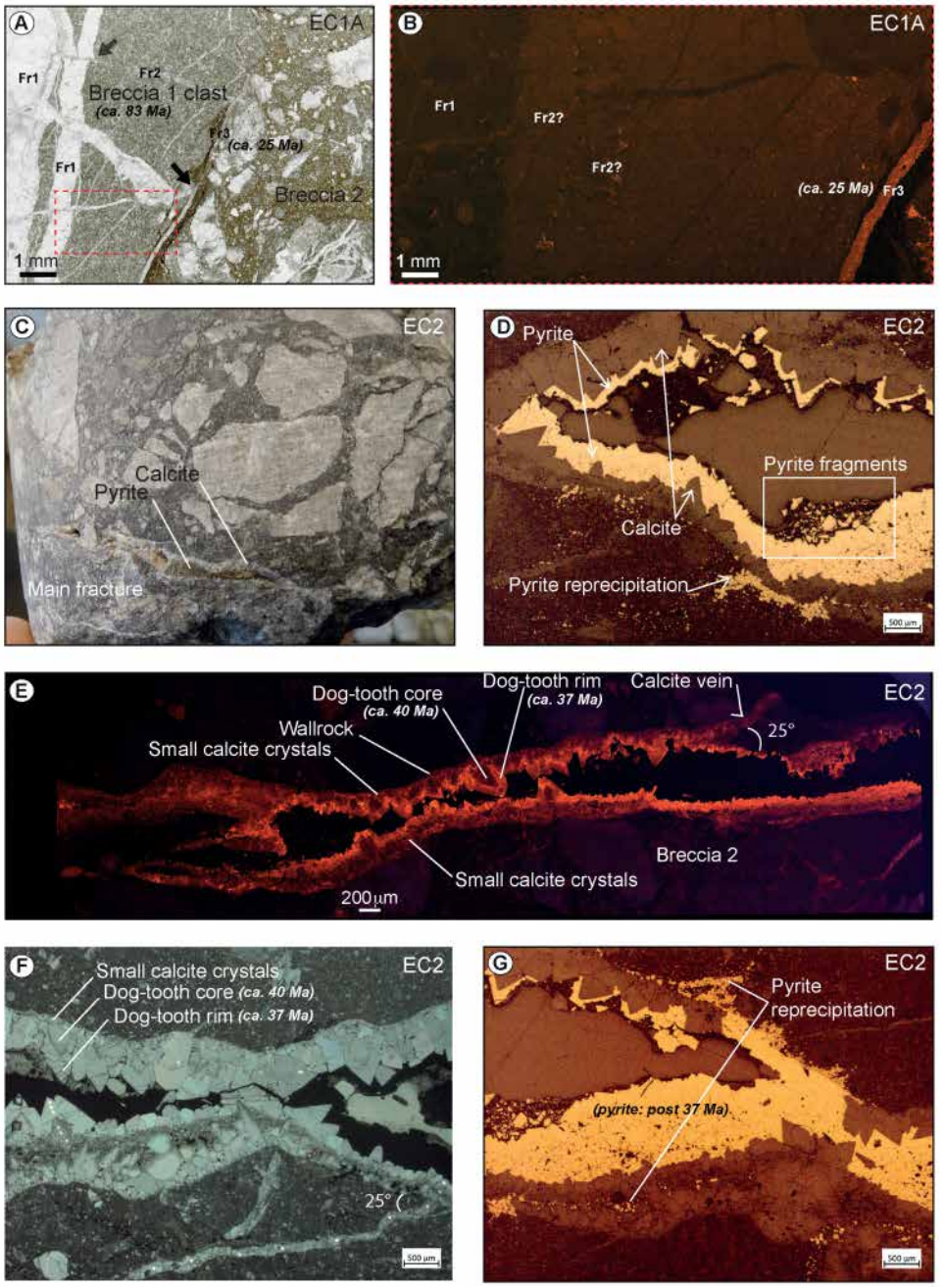


**Figure 3.** Microphotographs of thin sections from samples of the La Rouvière Fault Core. (A) Scan of the sample EC1A entire thin section showing the crosscutting relationships between fracture families and breccia phases. The left part of the image is a clast from breccia 1, (B) Close-up CL image showing the highly bright orange luminescence of Fr3 and crosscutting relationships with previous fractures and breccias, (C) EC2 sample showing main sigmoidal shape fracture filled by calcite and pyrite crystals at the scale of the hand specimen, (D) EC2 fracture filled with calcite and pyrite observed in reflected light. Note the pyrite crystals fragmentation at the bottom right, (E) Main EC2 fracture in cathodoluminescence image (CL), (F) Calcite growing episodes of main EC2 vein under cross polarized light, (G) Main and second phase of pyrite crystallization in reflected light. Note that U–Pb ages obtained in this study have been added on photographs for clarity.

to macro sparite suggesting to some degree that a phase of dissolution occurred. Also, these Fr3 fractures are not systematically cemented as they can occasionally contain pore spaces.

## 4. U–Pb geochronology

### 4.1. *U–Pb isotopes analytical methods*

U–Pb isotopes of carbonate minerals were determined by laser ablation inductively coupled mass spectrometry (LA-ICP-MS) with an ESI NWR193UC laser coupled to a Nu AttoM ES sector field ICP-MS at GeoRessources, Université de Lorraine. Key instrument parameters are included in the Supplementary Table 1 (Table 1 SX). Key laser operating conditions include a laser spot size of between 80–150 µm with 8 Hz repetition rate and between 2–4 J·cm$^{-2}$ energy density at the sample surface. The following masses were monitored with the respective dwell time (in microseconds) in parentheses: 202 (10), 204 (10), 206 (10), 207 (50), 208 (10), 232 (10), 235 (10), 238 (10). This configuration gives a total integration time of 0.1668 seconds for all masses. Raw data were processed in Iolite (v. 4) [Paton et al., 2011] using the UPb Combine DRS [Petrus and Kamber, 2012]. The WC1 calcite was used as the primary reference material for U/Pb ratios [assuming an age of 254.4 ± 6.4 Ma and $^{207}Pb/^{206}Pb_i$ of 0.85 ± 0.04; Roberts et al., 2017], and the NIST SRM614 for Pb/Pb ratios [assuming $^{207}Pb/^{206}Pb$ of 0.8710±0.008; Woodhead and Hergt, 2001]. The Duff Brown Tank limestone [U–Pb age of 64.07 ± 0.67; Hill et al., 2016] and the B6 calcite breccia [U–Pb age of 43.0±1.0 Ma; Pagel et al., 2018] were used to validate our reported ages. For all sessions (Supplementary Table 1 SY) we obtained a pooled lower intercept age of 63.42 ± 1.19 Ma (2s, $n$ = 62, MSWD = 1.5) for the Duff Tank Limestone, and 40.67 ± 0.55 Ma (2s, $n$ = 55, MSWD = 0.94) for the B6 calcite breccia. We report uncertainty at two levels for all samples in the form age $\pm x(y)$ Ma whereby $x$ is the measurement uncertainty, and $y$ includes an excess variance of 2.5% [estimated after Guillong et al., 2020] added to $x$ in quadrature. The concentration Pb (total of all isotopes), Th, and U were obtained using the Trace Elements DRS with the NIST614 [Jochum et al., 2011] as the primary reference material.

### 4.2. *U–Pb isotopes results*

U–Th–Pb concentrations and U–Pb isotope ratios are included in the Supplementary Table 1 (Table SZ). Rejected analyses are marked by an "$x$" in the data tables, and represented by an unfilled ellipse in Figure 4. These values were rejected for low concentrations leading to large measurement uncertainties.

All calcite minerals in this study have low and variable U between 0.013 and 13.50 ppm, and $Pb_{total}$ between 0.008 and 1.15 ppm. Thorium concentrations are typically below or at the limit of detection. However some samples show relative enrichment of up to 1.4 ppm. The range in U and $Pb_{total}$ of these carbonate minerals is like concentrations found in carbonates from a range of geological environments elsewhere including veins, diagenetic, biogenic and speleothem [e.g., Roberts et al., 2020].

All carbonate samples contain non-radiogenic Pb leading to discordant analyses on a $^{238}U/^{206}Pb$ vs. $^{207}Pb/^{206}Pb$ (a.k.a Terra-Wasserburg) diagram (Figure 4). Lower intercept ages and their uncertainties are included in the Supplementary Table 1 (Table Summary of ages) with the upper intercept initial Pb composition estimate, and the mean-square-weighted-deviation (MSWD) of the Discordia fit. Ages range from 87.7 ± 3.8 (4.4) Ma to 25.1 ± 1.7 (1.8) Ma with MSWD 1.3 or lower (Figure 5; Table 1). Upper intercept $^{207}Pb/^{206}Pb_c$ estimates are within the range of the terrestrial bulk Earth for their age [e.g. Stacey and Kramers, 1975] except for EC1A-Fr3, EC2A-Dog-tooth core, EC4A-Fr2 (vein 2) and EC5B-Fr1 (sigmoid) with values closer to ca. 0.75 and indicative of a more radiogenic common Pb isotopic composition.

## 5. Discussion

The core samples analysed in this paper were taken from the first hole drilled through the LRF which was reactivated during the 2019 Mw 4.9 Le Teil earthquake in France. This first drilling is part of the "HYPERDRILL" project aiming at reaching the focal depth of this recent earthquake to study rock mechanics and the impact of fluids on the nucleation and propagation of seismic ruptures [e.g. Paglialunga et al., 2023]. Here, our first goal was to reconstruct the long-term history of this deformation zone by applying LA-ICP-MS in situ calcite U–Pb geochronology on distinct generations of calcite-filled veins.

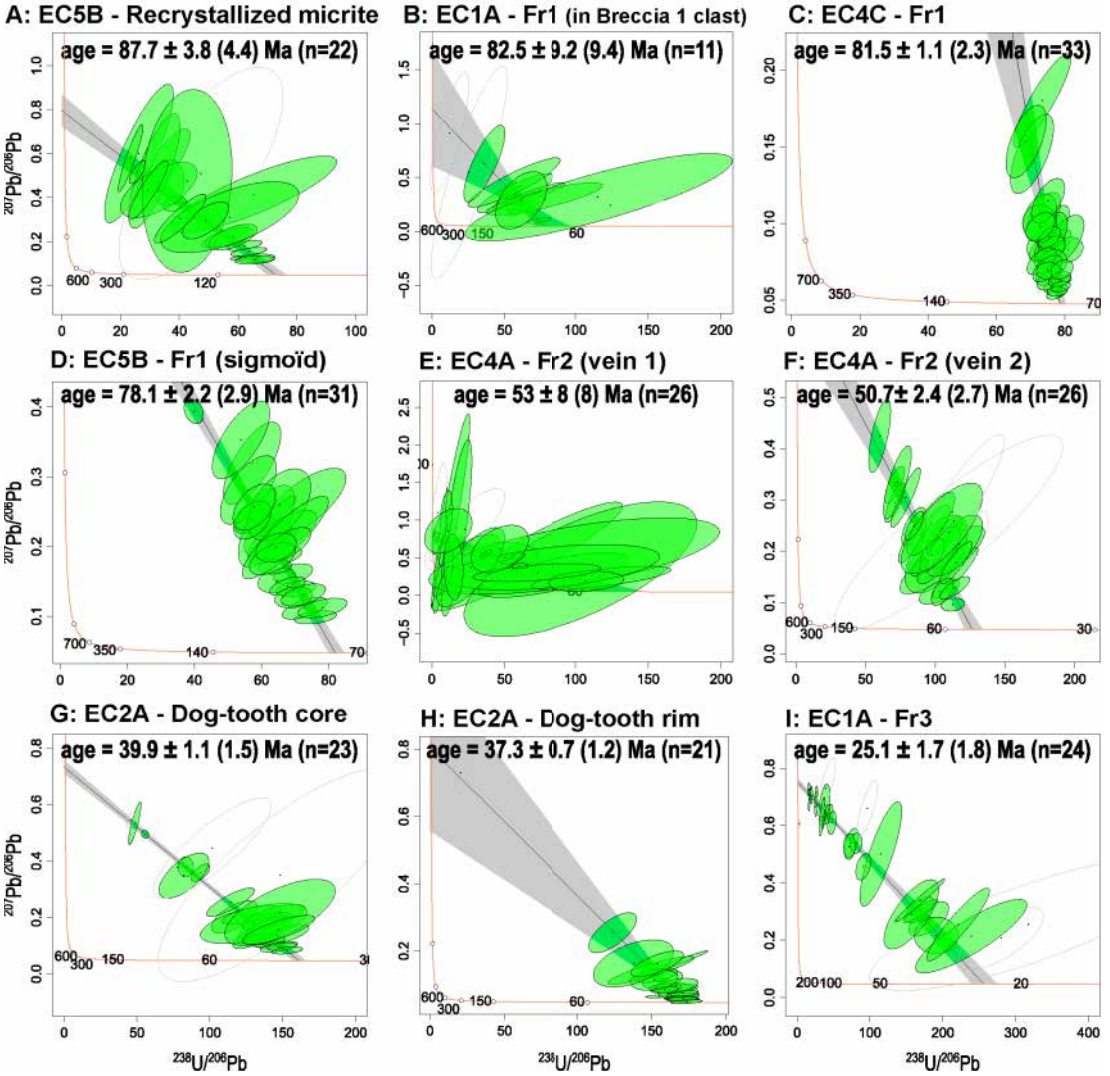


**Figure 4.** $^{238}U/^{206}Pb$ vs. $^{207}Pb/^{206}Pb$ (a.k.a Terra-Wasserburg) diagrams for all analysed sampled.

**Table 1.** Summary of U–Pb results

| Sample | $n$ | Age | 95% conf. | 95% conf. + $\varepsilon$ | $^{207}Pb^{206}Pb_c$ | 95% conf. | MSWD |
|---|---|---|---|---|---|---|---|
| EC1A—Fr3 | 24 | 25.1 | 1.7 | 1.8 | 0.755 | 0.013 | 0.99 |
| EC2A—Dog-tooth rim | 21 | 37.3 | 0.7 | 1.2 | 0.810 | 0.250 | 1 |
| EC2A—Dog-tooth core | 23 | 39.9 | 1.1 | 1.5 | 0.733 | 0.022 | 0.79 |
| EC4A—Fr2 (vein 2) | 26 | 50.7 | 2.4 | 2.7 | 0.711 | 0.089 | 0.93 |
| EC4A—Fr2 (vein 1) | 26 | 53.0 | 8.0 | 8.1 | 0.793 | 0.087 | 1.2 |
| EC5B—Fr1 | 31 | 78.1 | 2.2 | 2.9 | 0.741 | 0.052 | 1.2 |
| EC4C—Fr1 | 33 | 81.5 | 1.1 | 2.3 | 1.050 | 0.370 | 1.3 |
| EC1A—Fr1 | 11 | 82.5 | 9.2 | 9.4 | 1.140 | 0.530 | 1.1 |
| EC5B-Recrystal. micrite | 22 | 87.7 | 3.8 | 4.4 | 0.796 | 0.073 | 0.68 |

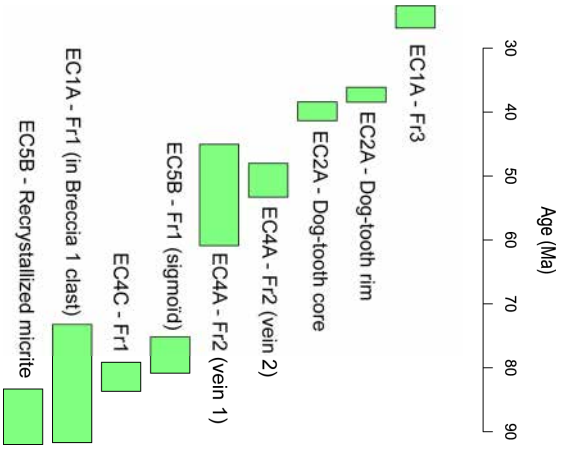


**Figure 5.** Summary of U–Pb ages with uncertainties.

### 5.1. *Relative versus absolute dating (Figure 6)*

Microstructural and relative chronology data from carbonate rocks of the LRF zone highlight four main tectonic events that have been bracketed by U–Pb geochronology between ~25 Ma and ~90 Ma (Figures 4 and 5; Table 1).

Microstructural analysis of representative calcite veins allows us to identify a first opening-mode fracture (Fr1) closely associated with angular clasts breccia 1 that we interpret to reflect extensional tectonics. These (micro)structures are superimposed by a second episode characterized by brecciated rocks (breccia 2) and fractures (Fr2) as well as shear deformation markers such as sheared stylolites and sigmoidal sheared-cracks that could be associated with a strike-slip fault kinematics on the LRF plane [e.g. Tondi et al., 2006]. Fracture filled by dog-tooth shape calcite crystals characterizing the EC2 sample developed after these two episodes. Finally, a last event is marked by open fractures Fr3 not systematically cemented that clearly cross-cut the previous structures.

When comparing these four key markers with in situ calcite U–Pb geochronology, we conclude that the LRF zone recorded the main tectonic events identified in the South-East basin of France: (1) both the Fr1 cements and sparite from recrystallized micrite have recorded U–Pb ages from ~90 to 75 Ma (Figures 2, 4 and 5; Table 1) that could be related to local extensional tectonics during the late Cretaceous where sedimentation was controlled by thermal subsidence in the Ardèche area inducing the migration of hanging wall of listric normal fault system to the east [Bonijoly et al., 1996], (2) Fr2 fracture-fill calcite cement yielded an age of ~50 Ma which is compatible with the later phase of the Pyrenean-Provence tectonic compression phase [e.g. Thomasset et al., 2024], (3) ages of ~40 and ~37 Ma from the EC2 sample obtained on dog-tooth core and rim, respectively, clearly indicate two stages of calcite crystallization within the EC2 fracture that may have opened during the early stage of the ESE–WNW extensional tectonics associated with the opening of Lion Gulf [Séranne et al., 2002] and to a larger extent with the European Cenozoic Rift System (ECRIS) [e.g. Dèzes et al., 2004], (4) the Fr3 fracture yielded an age of ~25 Ma that we interpret to reflect the ECRIS [e.g. Dèzes et al., 2004].

### 5.2. *The La Rouvière fault zone, a critical interface for fluid flow*

Cathodoluminescence images highlight contrasting carbonate families for each of the deformation markers. In calcite, luminescence is mainly controlled by the trace presence of $Fe^{2+}$ and $Mn^{2+}$ ions providing antagonistic effects [e.g. Scholle and Ulmer-Scholle, 2003] which in turn deliver information on the fluid chemistry from which the calcite formed. As a first approximation, early marine eogenetic cements generally display dull luminescence, whereas bright luminescence is often associated with deeper mesogenetic fluid or telogenetic meteoric diagenesis [e.g. Budd et al., 2000]. Based on these contrasted luminescence, we can state that the different calcite rich veins from the LRF zone have formed in the presence of different water composition, from sea water and/or meteoric to connate water. In addition, the crystallization of pyrite on the top of the ~40–37 Ma calcite minerals of the EC2 sample indicates that a fluid of different origin than marine and/or surface fluids invaded the LRF core after the main phase of dog-teeth calcite core and rim crystallizations. Based on the EC2 pyrite chemical composition, three different origins of fluids could be considered to explain pyrite precipitation. First, a local iron and sulfur enriched fluid (from intense pressure solution processes) that could have been stocked during the second phase of brecciation (breccia 2) and released in response to the Oligocene extensional

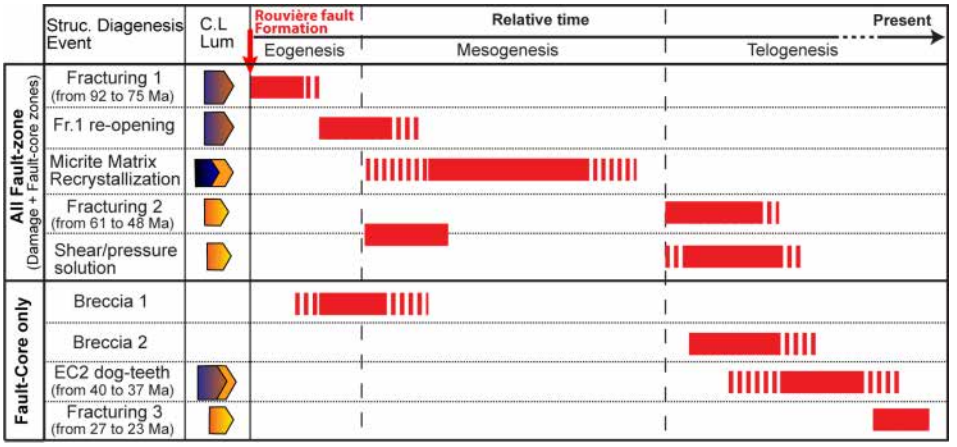


**Figure 6.** Chronological timeline linking the main identified (micro) structures to the structural diagenesis events. Note that U–Pb ages bracketing the main identified tectonic events have been mentioned.

tectonics. Second, a fluid sourced away from the fault core, which obtained the necessary iron and sulfur contents to precipitate pyrite crystals in the EC2 main fracture from the underlying organic matter-rich shale Valanginian formation [e.g. Berner, 1984]. Third, an allochthonous fluid that has become enriched with sulfur by passing through underlying Triassic evaporites [e.g. Laurent et al., 2021]. As demonstrated by the zoning of pyrite grains from EC2 revealed by electron microprobe analyses (Supplementary Figures 4 and 5 and Supplementary Table 2), a mixing of these different fluid sources could have been involved. Also, the zoned dog-tooth calcite minerals from the EC2 sample yielding two different ages (39.9 ±1.1 (1.5) Ma (core) and 37.3 ±0.7 (1.2) Ma (rim)) provide information on the kinetics of fracture cementation and sealing processes which, although being thought to last from centuries [Richard et al., 2015] to millions of years [Becker et al., 2010], have not been so far quantified. Here, our U–Pb results indicate that these processes can remain active during at least ~1 Ma.

Determining the fluids source that circulated in the La Rouvière deformation zone is beyond the scope of this paper. However, our study emphasizes the polyphase nature of the tectonic history recorded in the Le Teil area and points out that each tectonic episode has led to the formation of new structures and/or re-opening of fracture networks that enhanced porosity and permeability providing pathways for fluids to migrate and precipitate carbonate and/or pyrite.

### 5.3. *Summary of tectonic events recorded by the La Rouvière fault in the frame of the Cévennes Faults System*

The chronology and the kinematics of tectonic deformations along the Cévennes Faults System and the western boundary of the South-East basin of France have been constrained by geophysical investigations (seismic reflection profiles, deep drilling, structural modeling) and field observations [e.g. Roure et al., 1992, Bonijoly et al., 1996, Elmi et al., 1996, Martin and Bergerat, 1996, Marconato et al., 2022, Thomasset et al., 2024]. As mentioned above (Section 5.1), our U–Pb results highlight four main successive tectonic episodes which can be grouped into the following time intervals: (1) from ~90 to 75 Ma, (2) from ~60 to 50 Ma, (3) from ~40 to 37 Ma, and (4) ~25 Ma. We interpret these events to reflect (1) thermal subsidence during the late Cretaceous in the Ardèche region which is the western margin of the SE basin [Bonijoly et al., 1996], (2) the late-Pyreneo-Provençal deformation related to the N–S trending shortening of the South-East basin [Thomasset et al., 2024], (3) the opening of the Gulf of Lion which is also closely related to the ECRIS [e.g. Séranne et al., 2002, Dèzes et al., 2004], and (4) a middle to late stage of the ECRIS.

We note that our studied samples did not record the late Miocene–Pliocene tectonic episodes that have been documented by previous authors on different regional faults of the CFS [e.g. Bonijoly et al., 1996, Martin and Bergerat, 1996].

As shown by focal mechanisms and InSAR data [Ritz et al., 2020, Marconato et al., 2022], the LRF experienced a reverse faulting mechanism during the 2019 Le Teil earthquake which attests to the inversion of this long-lived normal fault system [Thomasset et al., 2024]. However, no morphotectonic evidence of previous significant compressional tectonic event has been identified in the field [Ritz et al., 2020]. This is in agreement with our microstructural data and related U–Pb results suggesting that the most recent tectonic event recorded by the LRF is 25.1 ± 1.7 (1.8) Ma old (Figures 4 and 5). This last event is very likely related to the extensional tectonic regime that developed in response to the ECRIS [e.g. Séranne, 1999, Thomasset et al., 2024].

Also, we note that E–W trending Miocene compressional tectonics related to Alpine tectonics and documented in different areas within the Rhône Valley [Bergerat, 1982, Blès and Gros, 1991] has not been recorded in our studied samples. However, this does not preclude the possibility that this event has not affected the Montélimar region as, although any geochronological data have been acquired, Martin and Bergerat [1996] have interpreted structures from the Balazuc borehole going through the Uzer fault further west and belonging to the CFS to record Alpine tectonics. The only event suggesting a potential LRF activity between ~25 Ma and 2019 is from a paleoseismology study from Ritz et al. [2022] mentioning a paleoearthquake at ca. 13.3 ka. This result highlights the very long quiescent period of a fault that has therefore not been identified as active [Jomard et al., 2017].

## 6. Conclusion

U–Pb geochronology on calcite within microstructures of core samples from the first exploratory drilling cross-cutting the La Rouvière fault plane (south-east part of France) highlighted four main tectonic events between ~90 and 25 Ma: (1) A late stage Cretaceous event (90–75 Ma) revealed by a first generation of opening fractures that formed coevally with the development of known regional listric synsedimentary faults during thermal subsidence of the Ardèche area, (2) An early Eocene event (~50 Ma) marked by a second fracture group that we interpret to reflect the late stage of the Pyrenean-Provence tectonic compression/transpression phase, (3) A mid to late Eocene episode (40–37 Ma) recorded by dog-tooth polyphase calcite crystals from major fractures that very likely occurred during the opening of the Gulf of Lion, and more widely, represent a consequence of the European Cenozoic Rift System (ECRIS) activity, and (4) A last event at 25 Ma recorded by narrow fractures cross-cutting all the above structures that we relate to the late stage of the ECRIS. Our studied samples did not record any compressional event associated with Alpine tectonics, neither any reverse fault mechanism from intraplate processes like that expressed by the Mw 4.9 2019 Le Teil earthquake.

The La Rouvière fault represents a key object to study the complex polyphase history of this part of Europe, and through the different nature of structures and minerals it offers, makes it a natural laboratory to study in the future the signature of fluids and fluid flow history.

From a seismic hazard point of view, this study suggests that the La Rouvière fault has had a very long period of inactivity, close to 25 Ma. Although long recurrence times are to be expected in an intraplate domain with a very low deformation rate, such a period of inactivity poses a challenge to the definition of active faults in this type of environment.

## Declaration of interests

The authors do not work for, advise, own shares in, or receive funds from any organization that could benefit from this article, and have declared no affiliations other than their research organizations.

## Funding

This study was funded through a BQR (Bonus Quality Recherche) project in 2023 from the Observatoire de la Côte d'Azur. The authors thank the CNRS/INSU project Tellus FREMTEIL for funding the drilling through La Rouvière fault and the company Sondafor for the drilling of the borehole.

## Acknowledgements

We appreciated and thank O. Parizot and C. Thomasset for fruitful discussions in the field. AG acknowledges support from GeoRessources. CM thanks

P. Léonide for his access to cathodoluminescence at the CEREGE laboratory. The authors thank Thin Section Lab for the quality of polished thin and thick thin sections, and also Idriss Friry and the TotalEnergies company for scanning the core samples. The authors thank the editorial team and acknowledge the careful remarks of an anonymous reviewer.

## Supplementary data

Supporting information for this article is available on the journals website under https://doi.org/10.5802/crgeos.280 or from the author.

## References

Becker, S. P., Eichhubl, P., Laubach, S. E., Reed, R. M., Lander, R. H., and Bodnar, R. J. (2010). A 48 m.y. history of fracture opening, temperature, and fluid pressure: Cretaceous Travis Peak Formation, East Texas basin. *Geol. Soc. Am. Bull.*, 122, 1081–1093.

Bergerat, F. (1982). Le couloir rhodanien au Paleogene : analyse de la fracturation et interprétation cinématique régionale. *Rev. Géol. Dynam. Géogr. Phys.*, 23(5), 329–313.

Berner, R. A. (1984). Sedimentary pyrite formation: An update. *Geochim. Cosmochim. Acta*, 48, 605–615.

Blès, J. L. and Gros, Y. (1991). Stress field changes in the Rhone Valley from the Miocene to the present. *Tectonophysics*, 194, 265–277.

Bonijoly, D., Perrin, J., Roure, F., Bergerat, F., Courel, L., Elmi, S., and Mignot, A. (1996). The Ardèche palaeomargin of the South-East Basin of France: mesozoic evolution of a part of the Tethyan continental margin (Géologie Profonde de la France programme). *Mar. Pet. Geol.*, 13, 607–623.

Boullier, A.-B. (2011). Fault zone geology: lessons from drilling through the Nojima and Chelungpu faults. *Geol. Soc. Lond. Spec. Publ.*, 359, 17–37.

Budd, D. A., Hammes, U., and Ward, W. B. (2000). Cathodoluminescence in calcite: New insights on Mn-activation, Fe-quenching, and sensitizing by Pb and Zn using synchrotron X-ray fluorescence. *J. Sediment. Petrol.*, 70, 217–226.

Causse, M., Cornou, C., Maufroy, E., Grasso, J. R., Baillet, L., and El Haber, E. (2021). Exceptional ground motion during the shallow Mw 4.9 2019 Le Teil earthquake, France. *Commun. Earth Env.*, 2, article no. 14.

De Novellis, V., Convertito, V., Valkaniotis, S., Casu, F., Lanari, R., Monterroso Tobar, M. F., and Pino, N. A. (2020). Coincident locations of rupture nucleation during the 2019 Le Teil earthquake, France and maximum stress change from local cement quarrying. *Commun. Earth Environ.*, 1, article no. 20.

Delouis, B., Oral, E., Menager, M., Ampuero, J. P., Guilhem Trilla, A., Régnier, M., and Deschamps, A. (2021). Constraining the point source parameters of the 11 November 2019Mw 4.9 Le Teil earthquake using multiple relocation approaches, first motion and full waveform inversions. *C. R. Géosci.*, 353, 493–516.

Dèzes, P., Schmid, S. M., and Ziegler, P. A. (2004). Evolution of the European Cenozoic Rift System: Interaction of the Alpine and Pyrenean orogens with their forland lithosphere. *Tectonophysics*, 389, 1–33.

Elmi, S., Busnardo, R., Clavel, B., Camus, G., Kieffer, G., Bérard, P., and Michaëly, B. (1996). *Notice explicative. Carte géologique de la France au 1/50000.* Bureau de Recherches Géologiques et Minières, Orléans. feuille Aubenas (865), 170p.

Guillong, M., Wotzlaw, J. F., Looser, N., and Laurent, O. (2020). Evaluating the reliability of U–Pb laser ablation inductively coupled plasma mass spectrometry (LA–ICP–MS) carbonate geochronology: matrix issues and a potential calcite validation reference material. *Geochronology*, 2(1), 155–167.

Hill, C. A., Polyak, V. J., Asmerom, Y., and Provencio, P. (2016). Constraints on a Late Cretaceous uplift, denudation, and incision of the Grand Canyon region, southwestern Colorado Plateau, USA, from U–Pb dating of lacustrine limestone. *Tectonics*, 35(4), 896–906.

Jébrak, M. (1997). Hydrothermal breccias in vein-type ore deposits: A review of mechanisms, morphology and size distribution. *Ore Geol. Rev.*, 12, 111–134.

Jochum, K. P., Weis, U., Stoll, B., et al. (2011). Determination of reference values for NIST SRM 610–617 glasses following ISO guidelines. *Geostand. Geoanal. Res.*, 35(4), 397–429.

Jomard, H., Cushing, E. M., Palumbo, L., Baize, S., David, C., and Chartier, T. (2017). Transposing an active fault database into a seismic hazard

fault model for nuclear facilities—Part 1: building a database of potentially active faults (BDFA) for metropolitan France. *Nat. Hazards Earth Syst. Sci.*, 17, 1573–1584.

Jomard, H., Scotti, O., Auclair, S., Dominique, P., Manchuel, K., and Sicilia, D. (2021). The SISFRANCE database of historical seismicity. State of the art and perspectives. *C. R. Géosci.*, 353(S1), 257–280.

Larroque, C., Baize, S., Albaric, J., et al. (2021). Seismotectonics of southeast France : from the Jura mountains to Corsica. *C. R. Géosci.*, 353, 105–151.

Laubach, S. E., Eichhubl, P., Hilgers, C., and Lander, R. H. (2010). Structural diagenesis. *J. Struct. Geol.*, 32, 1866–1872.

Laurent, D., Durlet, C., Barré, G., et al. (2021). Epigenic vs. Hypogenic speleogenesis governed by $H_2S/CO_2$ hydrothermal input and Quaternary icefield dynamics (NE French Pyrenees). *Geomorphology*, 387, article no. 107769.

Manchuel, K., Traversa, P., Baumont, D., Cara, M., Nayman, E., and Durouchoux, C. (2017). The French seismic CATalogue (FCAT-17). *Bull. Earthq. Eng.*, 8(16), 2227–2251.

Marconato, L., Leloup, P. H., Lasserre, C., et al. (2022). Insights on fault reactivation during the 2019 November 11, Mw 4.9 Le Teil earthquake in southeastern France, from a joint 3-D geological model and InSAR time-series analysis. *Geophys. J. Int.*, 229, 758–775.

Martin, P. and Bergerat, F. (1996). Palaeo-stresses inferred from macro- and microfractures in the Balazuc-1 borehole (GPF programme). Contribution to the tectonic evolution of the Cévennes border of the SE Basin of France. *Marine Pet. Geol.*, 13(6), 671–684.

Masson, C., Mazzotti, S., and Vernant, P. (2019). Precision of continuous GPS velocities 20 from statistical analysis of synthetic time series. *Solid Earth*, 10, 329–342.

Mort, K. and Woodcock, N. H. (2008). Quantifying fault breccia geometry: Dent Fault, NW England. *J. Struct. Geol.*, 30, 701–709.

Pagel, M., Bonifacie, M., Schneider, D. A., et al. (2018). Improving paleohydrological and diagenetic reconstructions in calcite veins and breccia of a sedimentary basin by combining Δ47 temperature, $\delta$18O water and U–Pb age. *Chem. Geol.*, 481, 1–17.

Paglialunga, F., Passelègue, F., Latour, S., Gounon, A., and Violay, M. (2023). Influence of viscous lubricant on nucleation and propagation of frictional ruptures. *J. Geophys. Res.: Solid Earth*, 128, article no. e2022JB026090.

Paton, C., Hellstrom, J., Paul, B., Woodhead, J., and Hergt, J. (2011). Iolite: Freeware for the visualisation and processing of mass spectrometric data. *J. Anal. At. Spectrom.*, 26(12), 2508–2518.

Petrus, J. A. and Kamber, B. S. (2012). VizualAge: A novel approach to laser ablation ICP–MS U–Pb geochronology data reduction. *Geostand. Geoanal. Res.*, 36(3), 247–270.

Richard, J., Doan, M.-L., Gratier, J.-P., and Renard, F. (2015). Microstructures induced in porous limestone by dynamic loading, and fracture healing: an experimental approach. *Pure Appl. Geophys.*, 172, 1269–1290.

Ritz, J. F., Baize, S., Cathelin, N., et al. (2022). Paleoseismological investigations of the La Rouvière fault, unexpected source of the 11-11-2019, Mw4.9 Le Teil surface rupturing earthquake (Cévennes fault system, France). In *Proceedings of the 11th International INQUA Workshop on Paleoseismology, Active Tectonics and Archaeoseismology ("PATA Days") 25–30 September 2022, Aix-En-Provence, France*, pages 189–192. https://zenodo.org/records/7736477#.ZCXHr3ZBw2w.

Ritz, J. F., Baize, S., Ferry, M., Larroque, C., Audin, L., Delouis, B., and Mathot, E. (2020). Surface rupture and shallow fault reactivation during the 2019 Mw 4.9 Le Teil earthquake, France. *Commun. Earth Env.*, 1, article no. 10.

Roberts, N. M., Rasbury, E. T., Parrish, R. R., Smith, C. J., Horstwood, M. S., and Condon, D. J. (2017). A calcite reference material for LA–ICP–MS U–Pb geochronology. *Geochem. Geophys. Geosyst.*, 18(7), 2807–2814.

Roberts, N. M. W., Drost, K., Horstwood, M. S. A., et al. (2020). Laser ablation inductively coupled plasma mass spectrometry (LA–ICP–MS) U–Pb carbonate geochronology: strategies, progress, and limitations. *Geochronology*, 2, 33–61.

Roure, F., Brun, J. P., Colletta, B., and Van den Driessche, J. (1992). Geometry and kinematics of extensional structures in the Alpine Foreland Basin of southeastern France. *J. Struct. Geol.*, 14, 503–519.

Roure, F., Brun, J. P., Colletta, B., and Vially, R. (1994). Multiphase extensional structures, fault reactiva-

tion, and petroleum plays in the Alpine Foreland Basin of Southeastern France. In Mascle, A., editor, *Hydrocarbon and Petroleum Geology of France*, pages 245–268. Springer, Berlin-Heidelberg.

Scholle, P. A. and Ulmer-Scholle, D. S. (2003). A color guide to the petrography of carbonate rocks: Grains, Textures, Porosity, Diagenesis. In *AAPG Memoir*, volume 77, pages 1–477. American Association of Petroleum Geologists, Tulsa, Oklahoma.

Séranne, M. (1999). The Gulf of Lion continental margin (NW Mediterranean) revisited by IBS: An overview. In Durand, B., Jolivet, L., Horvath, F., and Séranne, M., editors, *The Mediterranean Basins: Tertiary Extension within the Alpine Orogen*, volume 156, pages 15–36. Geological Society, London.

Séranne, M., Camus, H., Lucazeau, F., Barbarand, J., and Quinif, Y. (2002). Cretaceous to Quaternary Denudation-Sedimentation in the Cevennes and Languedoc (S. France): Reconstructing a Polyphase Evolution Using a Multidisciplinary Approach. In *STRATI 2002, 3ème congrès français de stratigraphie, Lyon, 8–10 juillet 2002*, Docum. Lab. Géol. Lyon, 2002, n° 156, pages 213–214.

Stacey, J. S. and Kramers, J. D. (1975). Approximation of terrestrial lead isotope evolution by a two stage model. *EarthPlanet. Sci. Lett.*, 26, 207–221.

Thomasset, C., Ritz, J. F., Pouliquen, S., Manchuel, K., and Le-Roux-Mallouf, R. (2024). Geometry and tectonic history of the north-eastern faults system (SE Basin, France): new insights from deep seismic reflection profiles. *BSGF - Earth Sci. Bull.*, 195, article no. 17.

Tondi, E., Antonellini, M., Aydin, A., Marchegiani, L., and Cello, G. (2006). The role of deformation bands, stylolites and sheared stylolites in fault development in carbonate grainstones of Majella Mountain, Italy. *J. Struct. Geol.*, 28, 376–391.

Vallage, A., Bollinger, L., Champenois, J., et al. (2021). Multitechnology characterization of an unusual surface rupturing intraplate earthquake: the ML 5.4 2019 Le Teil event in France. *Geophys. J. Int.*, 226, 803–813.

Woodhead, J. D. and Hergt, J. M. (2001). Strontium, neodymium and lead isotope analyses of NIST glass certified reference materials: SRM 610, 612, 614. *Geostand. Newslett.*, 25(2–3), 261–266.